Elementary Loading Processes (ELP) involved in breaking wave impacts: findings from the Sloshel project

W. Lafeber[1], *L. Brosset*[2], *and H. Bogaert*[1]

[1]*MARIN, Hydro Structural Services, Wageningen, the Netherlands*
[2]*GTT (Gaztransport & Technigaz), Liquid Motion Department, Saint-Rémy-lès-Chevreuse, France*

ABSTRACT

MarkIII is one of the containment systems designed by GTT for LNG storage or transportation. It features a corrugated stainless steel membrane which modifies locally the flow of LNG in the tanks of LNG carriers, hence modifies the loads during sloshing impacts.

The interactions between breaking waves and the MarkIII corrugated membrane were described in Bogaert, Brosset and Kaminski (2010). The observations were based on the *large scale* impact tests of the Sloshel project performed in 2009. In this paper, these interactions are described again but based this time on the Sloshel *full scale* impact tests performed in 2010. In both test campaigns, unidirectional breaking waves were generated in flume tanks in order to break onto instrumented walls. Full scale tests were performed with a water height at rest of 4 m and the wall was covered by the real MarkIII membrane. Large scale tests were performed at scale 1:6, including the corrugated surface covering the wall, mimicking accurately the MarkIII membrane. In both cases pressure sensors were positioned in between the corrugations. Special sensors were designed to measure the forces on corrugations. The wave-corrugation interactions were captured by high speed cameras synchronized with the data acquisition system.

Qualitatively, the interactions observed at full scale are very similar to those observed at scale 1:6. However, full scale measurements allow a more in depth analysis of the local phenomena involved. The paper shows that the different kinds of interactions between breaking waves and either a flat or a corrugated wall induce loads that are combinations of only a few *Elementary Loading Processes* (ELPs): 1. direct impact, 2. building jet along the wall from the impact area and 3. compression/expansion of entrapped or escaping gas. In case of a corrugated wall, additional combinations of ELPs occur because new local flow situations intervene. However, these are still combinations of the same ELPs. Therefore, the ELPs are considered as the building blocks of any load on a wall impacted by a wave.

INTRODUCTION

The MarkIII membrane Cargo Containment Systems (CCS) is mainly composed of 3 m x 1 m panels of polyurethane foam covered by a stainless steel corrugated membrane in contact with the LNG at -162°C (see Figure 1). The membrane features large parallel corrugations crossing perpendicular small parallel corrugations. The large and small corrugations are respectively 54 mm and 37.2 mm high. The distance between two large or two small corrugations is 340 mm.

FIGURE 1: Primary membrane of the MarkIII CCS, reinforced version.

On the longitudinal walls of the MarkIII tanks the large corrugations are vertical whilst they are horizontal on the transverse bulkheads.

Deformations of the membrane corrugations are sometimes observed on board MarkIII ships during dry dock inspections. These deformations, without any leakage of the cargo, affect both large and small corrugations mainly in the corners of the ceiling and less frequently in the region covering a few meters above the lower chamfers of the longitudinal bulkheads. They are obviously caused by sloshing impacts. Some corrugations are globally bent whereas some others are pinched almost symmetrically.

Although it has been proved that the deformations of the corrugations do not affect their thermo-mechanical behavior nor their lifetime, any piece of information helping to understand the influence of the corrugations on the loading mechanisms is welcome. Qualitative and quantitative results have been drawn on this matter from different wave impact test campaigns of the Sloshel project. This paper focuses on the qualitative aspects, namely on a phenomenological comparison between loads induced by breaking waves on a flat and a corrugated wall. The quantitative results are described in another paper (see Marhem et al. (2012)).

Three wave impact test campaigns were performed in two different flume tanks within the Sloshel project: full scale NO96 tests were carried out without the primary membrane (see Brosset et al. (2009)); scale 1:6 tests, so-called *large scale* tests, were performed with a flat and corrugated wall configuration (see Bogaert, Brosset and Kaminski (2010)) and full scale MarkIII tests were carried out with the primary membrane (see Kaminski and Bogaert (2010b)). The results presented in this paper refer to large scale tests for results on a flat

wall and to full scale MarkIII tests for results on a corrugated wall. The full scale N096 database has not been used for the description of wave/flat wall interactions although these tests were performed without membrane, hence with a flat wall, because no accurate high speed videos of the last stages of the waves shape had been recorded at that time.

During one of the last tests of the full scale MarkIII test campaign, a flip-through impact was intentionaly created in order to induce very large local impact pressures. The corrugations were deformed up to 5 mm. Results derived from this very test, including the loads on the deformed corrugations are presented in a specific paper (see Brosset et al. (2011)).

After a short description of the test set-ups, the differences between wave impacts on a flat and corrugated wall are shown through a selection of representative wave impacts. The loads induced by the waves, whatever the kind of wall surface, turn out to result from different combinations of the same Elementary Loading Processes (ELP). The different ELPs, therefore considered as building blocks of any wave impact load, and the different combinations of ELPs that occur on a flat and on a corrugated wall are listed and characterized.

WAVE IMPACT TESTS

Full scale MarkIII tests

The full scale MarkIII tests were carried out in the Delta flume of Deltares (NL). The flume is 7 m high and 5 m wide. A transverse test wall was placed 145 m from the piston-type wavemaker. The test wall and the set-up are detailed by Kaminski and Bogaert (2010b). The test wall was completely covered by the MarkIII membrane as shown in Figure 2. The large corrugations were set vertically. This choice was motivated by the fact that most of the deformed corrugations observed in the lower part of the tanks on board LNG carriers were located on the longitudinal bulkheads. As the density of water used in the flume is more than twice the density of LNG, the reinforced version of the MarkIII membrane was used. In this version, installed recently on board some MarkIII ships, the large corrugations have ribs and all corrugations are strengthened with wooden wedges.

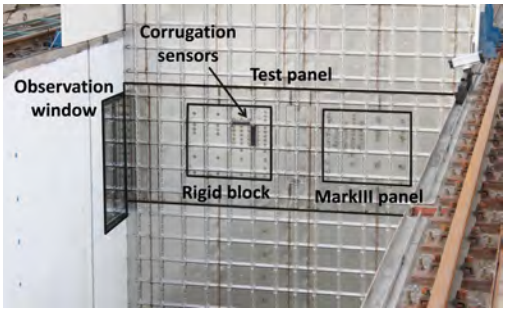

FIGURE 2: Test set-up of full scale MarkIII tests. Position of test panel, rigid block, MarkIII panel, corrugation sensors and window.

A steel test panel was embedded in the test wall which included a rigid block and a MarkIII panel. Their locations are indicated in Figure 2. Both the rigid block and the MarkIII panel were covered with the MarkIII membrane. Only the rigid block is considered in this paper. A detailed view is given in Figure 3. More information on the MarkIII panel can be found in Kaminski and Bogaert (2010b).

The rigid block was 1.2 m wide and 1 m high. It was instrumented mainly with 52 pressure sensors and two corrugation sensors. The data acquisition system for the pressure sensors and the corrugation sensors was sampling at 50kHz.

Pressure transducers with a sensitive membrane of 1.3 mm in diameter were used. The sensors were placed in larger sensor houses.

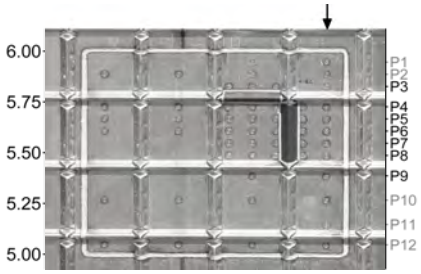

FIGURE 3: Detailed view of rigid block indicating pressure sensors and the vertical and horizontal corrugation sensors. The column of sensors that is used within this paper is indicated with the arrow. Heights are given in meters from the bottom of the flume.

The pressure transducers and the sensor houses are described by Kaminski and Bogaert (2010a). For the sake of clarity only pressure sensors P3 to P9, located on the right side of the rigid block are referred to in this paper. They formed a column of fully working pressure sensors around the horizontal corrugations located at 5.44 m and 5.78 m from the bottom of the flume.

The vertical and the horizontal corrugation sensors, developed by MARIN, had the shape of a corrugation and were put on the rigid block instead of the real corrugations. Each sensor measured two forces exerted on its corrugation. The forces on the lower and the upper sides of the horizontal corrugation sensor or the forces on the left and right sides of the vertical corrugation sensor were measured separately in the direction parallel to the wall. The signs were positive towards the centre of the corrugation. The location of the corrugation sensors is indicated on Figure 3.

An observation window was installed in one longitudinal wall of the flume, adjacent to the impacted wall, at the same height as the test panel. The window was 1.5 m high and 1 m wide and can be clearly seen in Figure 2. Behind the thick glass of the observation window, three high speed video cameras, synchronised with the data acquisition system, were installed. These cameras captured the shape of the waves during impacts. The first camera recorded the full view, the second camera focused on the area in between the horizontal corrugations at respectively 5.44 m and 5.78 m. The third camera made a close up view on the horizontal corrugations at 5.78 m, i.e. the row of the horizontal corrugation sensor. In this paper use will be made of the second and third camera recordings, which sampled respectively at 5 kHz and 1.2 kHz.

Large scale tests

The large scale tests were carried out in the Scheldt flume of Deltares (NL) in order to mimic the full scale tests at scale 1:6. The Scheldt flume is 55 m long, 1.5 m high and 1 m wide. The flume can be filled up to 1.0 m. The lateral flume walls are transparent. A piston wave maker is installed at one end of the flume. A rigid test wall was set-up at 23.7 m from the piston. The test wall and the whole set-up are detailed by Kaminski and Bogaert (2010b). The test set-up is shown in Figure 4.

A cover plate covered the entire surface of the test wall. Two configurations of the cover plate were tested successively: a flat cover plate and a cover plate with corrugations accurately mimicking the MarkIII membrane corrugations at scale 1:6 (see Figure 5). Two instrumented rigid test blocks were embedded into the test wall at scaled locations with regards to the two test blocks of full scale test wall. Pressure sensors P1 to P8, located on these blocks, are used in this study, see Figure 5. The data acquisition for the pressure sensors was sampling at 50 kHz.

High speed cameras synchronized with the data acquisition system filmed the waves just in front of the impacted wall through one of

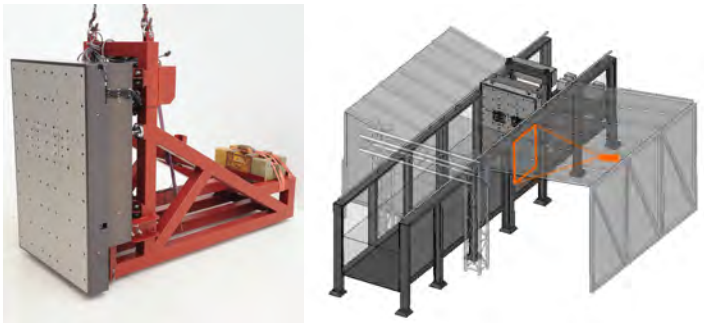

FIGURE 4: Test set-up at large scale. Rigid test wall alone (left) and installed in the flume (right).

the lateral transparent walls, sampling at 5 kHz. Figure 4 shows the shelters mounted on both sides of the flume near the wall in order to protect both the lighting system and the cameras from the splashes.

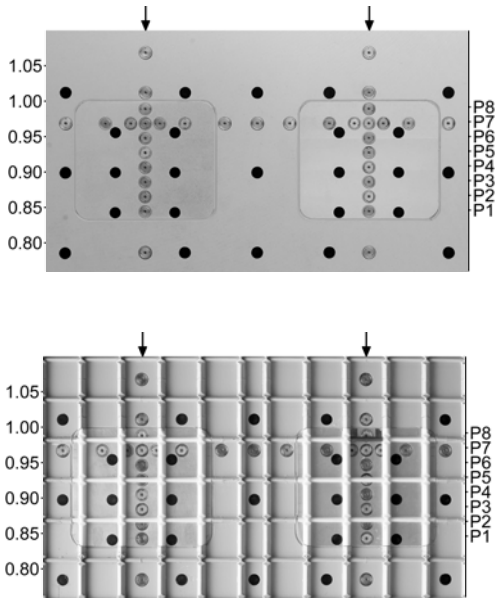

FIGURE 5: Detailed view of flat (top) and corrugated (bottom) cover plate at large scale indicating pressure sensors. A combination of sensors from the left and the right column, indicated with the arrows, is used in this paper. Height is given in meters from the bottom of the flume. The vertical spacing between the pressure sensors is 21mm.

Wave impact types

The breaking waves presented in this paper were generated by a wave focusing technique without bathymetry (Kimmoun et al. (2010)). Wave packets were generated by a piston in order to meet at a theoretical focal point. The way the resulting wave interacts with the wall changes gradually by slightly shifting the focal point location. Three impact types can be defined: slosh impact (see Figure 6), flip-through impact (see Figure 7) and air pocket impact (see Figure 8).

A *slosh impact* takes place when the focal point is behind the wall. The wave trough moves up along the wall and reaches the anticipated impact zone before the wave crest, preventing any impact of the crest. The speed and acceleration of the trough depend on the proximity of the forward moving wave front. As the wave front gets closer, the trough is accelerated and at some point, a vertical jet may build up, as seen in Figure 6 at instant t_2. An *air pocket impact* occurs when the wave breaks before the wall. The crest overturns while at the same

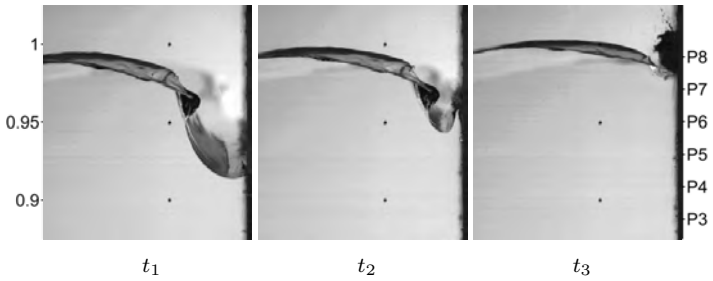

FIGURE 6: Slosh impact at three different instants. Time step equals 4 ms. Height given in meters.

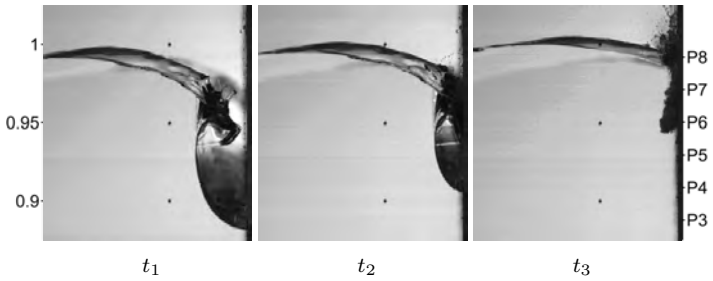

FIGURE 7: Flip-through impact at three different instants. Time step equals 4 ms. Height given in meters.

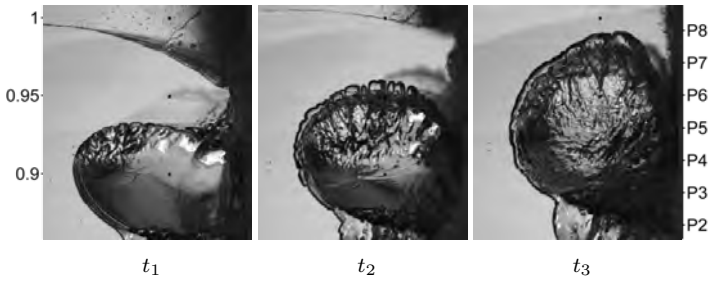

FIGURE 8: Air pocket impact at three different instants. Time step equals 8 ms. Height given in meters.

time the trough moves upward along the wall. When the crest impacts the wall, an air pocket is entrapped between the breaking wave and the wall, see Figure 8. A *flip-through impact* occurs when the wave crest and the wave trough converge towards a very small area at the wall. During the convergence, either the crest will break, which is the case for Figure 7 or a jet originating from the trough will start. Only a small range of focal point locations results in this convergence just in between the range for air pocket impacts and the range for slosh impacts. The flip-through can therefore be considered as a limit case between an air pocket and a slosh impact. The boundary between these different kinds of impact is not precisely defined.

Depending on the wave impact type the wall can be loaded by three wave parts: the wave trough, the impinging crest and the possible entrapped air-pocket. First, the interactions between these wave parts and the flat wall are described. After that, the corrugated wall is considered, where the wave parts interact in addition with the corrugations.

WAVE IMPACTS ON A FLAT WALL

In this section only the large scale database for the configuration with the flat cover plate will be used. The different observations will be illustrated by means of the three wave impacts shown in Figure 6, Figure 7 and Figure 8 at three instants t_1, t_2, t_3. The pressure signals recorded at sensors P1 to P8 for these three impacts are gathered in Figure 9, respectively in columns (a), (b) and (c). Instants t_1, t_2 and t_3 are indicated on the time traces.

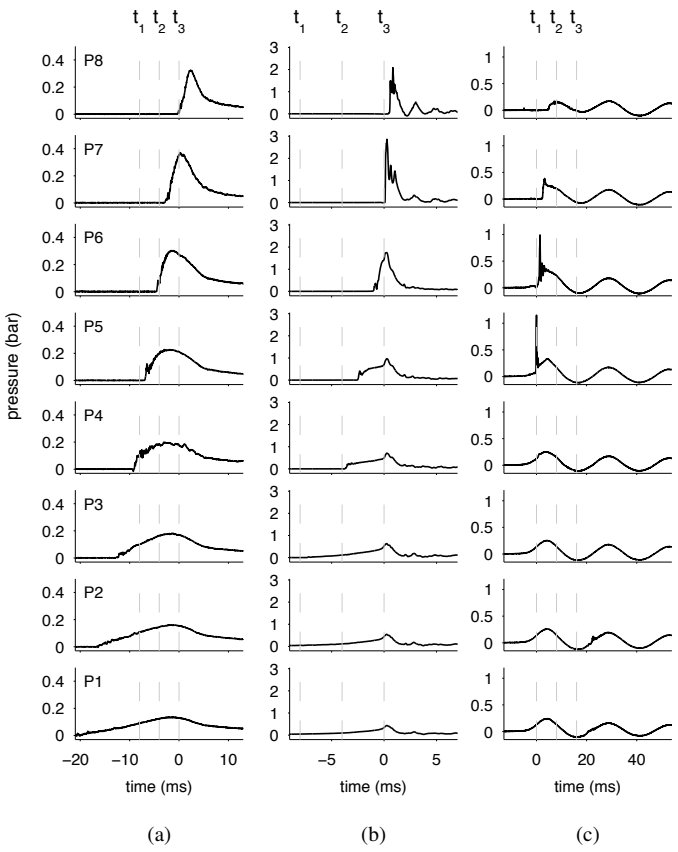

FIGURE 9: Pressure time traces at sensors P1 to P8 for impacts shown in Figure 6 (a), Figure 7 (b) and Figure 8 (c). Time scale and pressure scale are different for (a), (b) and (c).

Loads induced by the wave trough

Whatever the wave type considered, when a wave approaches a wall, its trough moves upward along the wall. This run-up process is very general and allows a transfer of a part of the horizontal momentum of the approching wave to a vertical momentum. This transfer is a mitigating process because it decreases the kinetic energy involved during the impact. As long as the wave front remains far enough from the wall, this run-up process is smooth: the trough remains locally horizontal at the contact point with the wall and the pressures induced onto the wall are insignificant. When the wave front is close enough - these conditions have been called *restricted trough* in Bogaert, Brosset and Kaminski (2010) - the run-up is much faster, it is even accelerated and the pressures on the wall increase. These restricted trough conditions are obtained for conditions close to flip-through impacts including small air-pocket impacts or sharp slosh impacts. The limit condition of flip-through induces the largest accelerations of the trough and also the largest pressures on the wall. The speeds of the trough run-up for the three impact types can be roughly compared thanks to Figure 6, Figure 7 and Figure 8, looking at the trough locations at the three instants t_1, t_2 and t_3. The trough is clearly moving faster in Figure 7, a flip-through impact, than in Figure 6, a sharp slosh impact, and much faster than in Figure 8, a large air-pocket impact. When the trough becomes restricted, a vertical upward jet builds up from the trough (see Figure 6 at t_2 and t_3 and Figure 7 at t_3).

The loads induced on the wall during the run-up process are hydrodynamic loads, only related to the local change of momentum direction. In the column (a) of Figure 9, the pressure signals recorded from P1 to P8 for the sharp slosh impact described in Figure 6 are entirely induced by this local phenomenon. One can follow the instant the trough reaches each sensor as the instant when the pressure starts to increase. As the trough is becoming more and more restricted, the pressure rise time is becoming shorter and the maximum pressure larger. In the column (b) giving the pressure signals for the flip-through impact shown in Figure 7, the part of the pressure signals from P1 to P5 before instant t_3, is also due to the change of momentum direction. At P4 and P5, there is a clear discontinuity in the pressure slope which corresponds to the building jet passing by the sensor.

This Loading Process is very general and thus will be present in other impact situations. It is for example the only loading process in case of a drop test of a wedge into a liquid initially at rest. Therefore it is considered as an *Elementary Loading Process* (ELP). It will combine with others ELPs to form composite loads. As it is significant only when a jet is building up along the wall, it will be named *Building jet ELP*, or simply ELP2, throughout this paper. As ELP2 is governed by the change of direction of the liquid velocities in front of the wall, the sharper this turn happens, the larger the pressures.

Loads induced by the wave crest

A wave crest starts overturning before the wall for a large range of focal point locations located ahead the wall. As far as the loads are concerned, three stages of development can be distinguished for the crest: (1) the approach; (2) the initial contact with the wall; (3) the formation of two vertical jets, upwards and downwards along the wall, from the contact area.

During the approach, the flow of the escaping gas has a major influence. A small but not insignificant part of the crest momentum is transferred to the gas. The velocity of the escaping gas can reach values as high as 50 m/s at full scale. The gas flows along the free surface and makes it very perturbed, extracting multiple drops of water and turning the free surface area into a spray. This phenomenon is referred to as the Kelvin-Helmholtz free surface instability (Drazin and Reid (2004)). It is believed to be the main cause of variability for pressure measurements during liquid impacts. An example of such perturbation of a crest free surface by a strong flow of escaping gas at full scale is shown in Figure 14 for instant t_1. This Figure will be introduced in the next section as it describes a wave impact on a corrugated wall.

Because of this perturbation of the free surface, there are multiple local contact points beween the bulk of water and the wall. At each of these points there will be a discontinuity of normal velocity just before and just after the contact that can be released only by emitting pressure waves into the water or strain waves into the wall. This loading process is very local but could theoretically lead, in certain conditions, to the acoustic pressure for a rigid wall. Each time a crest impacts a wall, this Loading Process is expected to appear in the close vicinity of the impact area. This ELP is named *Direct impact ELP*, or simply ELP1, throughout this paper.

Just after the direct impact the crest deflects upward and downward and two vertical jets are formed along the wall from the impact area. The liquid has to make sharp turns. This change of momentum direction induces loads on the wall. This loading process is the same as the one which develops for restricted wave trough conditions and has already been presented in the previous sub-section. This is again ELP2.

Figure 8 and column (c) of Figure 9, respectively give the shape and the pressure profile for an impacting wave crest. At instant t_1, the wave shape is given when there is a first contact happening close to sensor P5. A sharp peak of pressure can be observed on the pressure signal at P5 at instant t_1. This is ELP1. At P6, just a few milliseconds after t_1, thus clearly after the direct impact, the sharp peak that is observed is the consequence of the upward building jet from the crest, namely ELP2. A fraction of second later, the building jet reaches the location of sensor P7 which signal shows also a sharp rise, though less pronounced.

Figure 7 and column (b) of Figure 9 give respectively the shape and the pressure profile for a flip-through impact which is actually a small air-pocket impact. The pressure signals at P1 to P6, before instant t_3, have already been described as a consequence of the building jet from

the restricted trough, namely ELP2. It is now possible to explain the sharp peak of pressure at P7 by the direct impact of the crest (ELP1) at t_3 and a few millisecond later the peak pressure at P8 as the consequence of the upward building jet from the crest (ELP2).

When there is a direct impact (ELP1), a discontinuity of velocity has to be released locally. Actually, it means that all the flow around has to be adapted quickly and progressively to the new situation after the impact. This is done through the propagation of a shock wave at the speed of sound: the pressure peak is therefore propagated through the liquid, including along the wall. As the pressure waves are spherical, there is a quick attenuation of the amplitude with the distance. This propagation of the pressure peak induced by the direct impact at P7 is clearly observed a fraction of second after t_3 by the sensors below P7.

The local pressure peak induced by a direct impact (ELP1) always has a remote influence, though quickly damped, due to a shock wave. Most of the time, the pressure sensors will capture the remote influence of ELP1, instead of its very local maximum peak. Conversely, the building jet ELP (ELP2) is associated with the progressive change of momentum direction. It may be very sharp locally but at any time the flow around is well adapted and no shock wave is to be generated. Therefore, whatever the intensity of a pressure pulse induced by ELP2, it is travelling along the wall with the root of the jet but never generates a remote influence propagating at the speed of sound.

An impinging crest is the source of a direct impact loading, namely ELP1. The initial impact conditions (approaching phase) are strongly influenced by the flow of escaping gas which is at first approximation governed by the density ratio between the gas and the liquid. After the approaching phase has taken place, ELP1 is governed by the compressibility of the liquid and the elasticity of the impacted structure. For a crest impact, ELP1 is always strongly associated with ELP2 (building jet ELP).

Loads induced by the entrapped air pocket

In a flume, the conditions of an air pocket entrapment happen for a large range of focal point locations. The air pocket closes when the crest hits the wall. At this time the pressure inside is the atmospheric pressure unless the gas was already compressed during the escaping phase of the gas. The pocket is compressed mainly by the forward move of the wave front and the run-up of the trough. It essentially acts like a spring due to the compressibility of the air. Therefore, the pocket volume oscillates together with its internal pressure which remains almost uniform at each instant. A global upward motion of the pocket is imposed by the trough run-up. The maximum pressure inside the pocket and the frequency of oscillation increase for impacts involving decreasing entrapped volume of air, as already noticed in Bogaert, Brosset and Kaminski (2010) and in Kimmoun et al. (2010).

A large air pocket is entrapped for the wave impact shown in Figure 8. The pressures signals recorded by sensors P1 to P8 are given in column (c) of Figure 9. At time instant t_1, the crest impacts the wall. The impact of the crest occurs in the vicinity of pressure sensor P5. The air pocket encloses P2 to P4. Therefore the pressure signals for these sensors are the same. It corresponds to smooth damped oscillations. The pressure starts to increase on sensors P2 to P5 before instant t_1, namely while the gas is still escaping. The time evolution of the air-pocket pressure is in opposite phase with the volume as can be checked at instant t_3 for which the volume of the pocket is maximum and the pressure minimum. It can also be observed that the pressure goes below the atmospheric pressure during the expansion phase of the pocket. All points of the wall that are inside the air pocket are loaded by the air pocket pressure. Its influence is also felt by the points on the wall below the air pocket and the points on the wall inside the crest. The intensity depends on the distance to the air pocket as it ensures a continuity between the air pocket pressure and the ullage pressure. This remote influence can be clearly seen at P1 which is always outside the air pocket but measures almost the same pressure time history as within the pocket. Above the air pocket, this remote influence can be seen from P5 to P8, which are outside the pocket before instant t_2.

The loading process induced by the pulsating entrapped gas pocket is very general and will be encountered whenever an entrapped gas pocket or bubble will be in contact with the wall. It is considered as an ELP which is named *Pulsating gas pocket ELP*, or simply ELP3, throughout this paper. Subcategories could be defined depending on whether the gas is compressed while still escaping or while entirely entrapped. The governing phenomenon remains the compressibility of the gas.

WAVE IMPACTS ON A CORRUGATED WALL

In this section the full scale MarkIII database will be used to show the interactions between the wave parts and the corrugations of a MarkIII membrane covering an impacted wall. The same three impact types can be identified on a corrugated wall as on a flat wall: the slosh impact illustrated by Figure 10, the flip-through impact illustrated by Figure 12 and the air pocket impact illustrated by Figure 14. The pressure signals recorded at sensors P3 to P9 and the force exerted on the lower side of the horizontal corrugation sensor during these three wave impacts are respectively shown in Figure 11, Figure 13 and Figure 15. During these impacts on the corrugated wall the same wave parts interact with the wall as for the corresponding impacts on the flat wall. However, the way the trough, the entrapped air pocket and the crest interact with the wall becomes different. These interactions are additional combinations for the ELPs *direct impact*, *building jet* and *pulsating entrapped air* introduced in the previous section.

Loads induced by the wave trough

Whatever the type of wave impact, when the trough runs up along a corrugated wall it encounters horizontal corrugations. After the trough hits a corrugation, the flow separates from the wall and reattaches to the wall above the corrugation under the action of the forward moving wave front. The reattachment after the separation leads to the entrapment of a small air pocket above the corrugation. These processes of separation and reattachment are more or less violent depending on the restriction of the trough.

For the slosh impact of Figure 10, the wave front approach gives birth rather smoothly to a large jet of liquid running up along the wall. This global flow is perturbed by the local successive separations and reattachements induced by the corrugations. The local trough is delayed with regards to the tip of the tongue. The reattachment after separation from the lower corrugation occurs just underneath P7, just after t_1, but is soft. No peak pressure is detected on pressure signal of P7 in Figure 11. It is insignificant because the main direction of the flow in front of the wall is vertical. This soft reattachment is confirmed by the pressure signal of sensor P8. This sensor is located inside the small air pocket created above the lower corrugation by the reattachment but almost no compression is recorded in between t_1 and t_2. After this reattachment no local jet can be detected from the first contact location. The first rise of the pressure recorded successively by sensors P7, P6 and P5 is to be imputed to the building jet ELP (ELP2) but of the global flow. It would have been recorded, likely even more pronounced, without the interactions of the flow with the corrugations.

For the flip-through impact of Figure 12, the trough is significantly restricted by the presence of the close wave front. The reattachment of the flow to the wall after separation from the lower corrugation is very violent. It happens close to sensor P7 around t_3 with a horizontal velocity evaluated at 15 m/s from the videos. The signal recorded at P7 at this moment presents a very sharp peak with a maximum value larger than 40 bar and a duration shorter than 0.5 ms. This peak is the consequence of a *direct impact* ELP (ELP1). Sensor P8 is located inside the small air pocket entrapped above the lower corrugation by the reattachment. This pocket is clearly distinguishable on the image taken at t_3. Sensor P8 records a compression immediately after

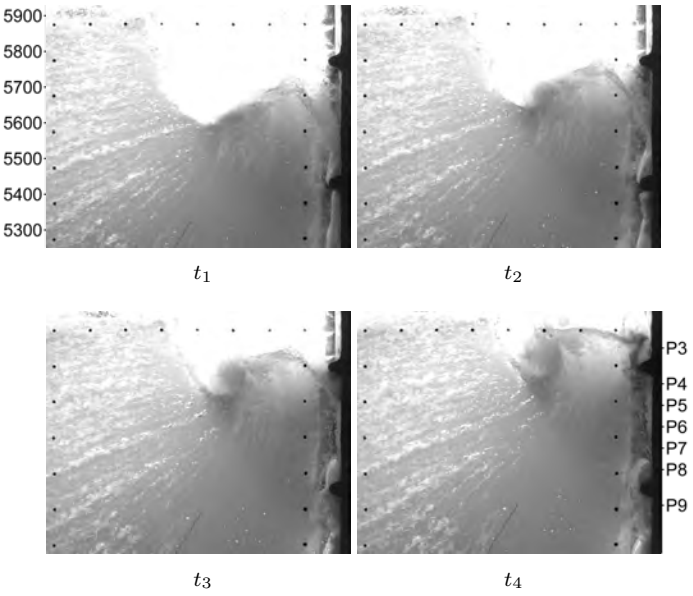

FIGURE 10: Slosh impact on corrugated wall at four different instants. Time step equals 5 ms. Height given in millimeters.

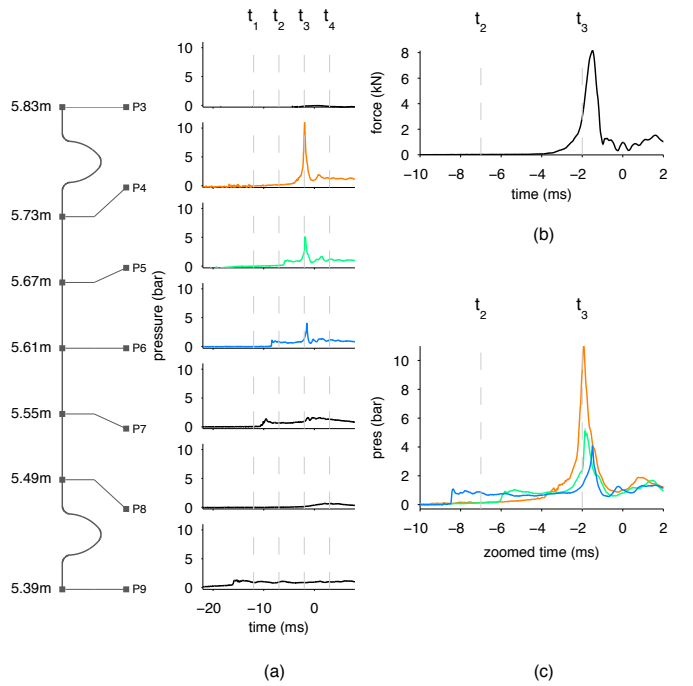

FIGURE 11: (a) Pressures, (b) Force on the bottom side of the horizontal corrugation in upward direction, (c) Zoom of pressures at sensors P4, P5 and P6.

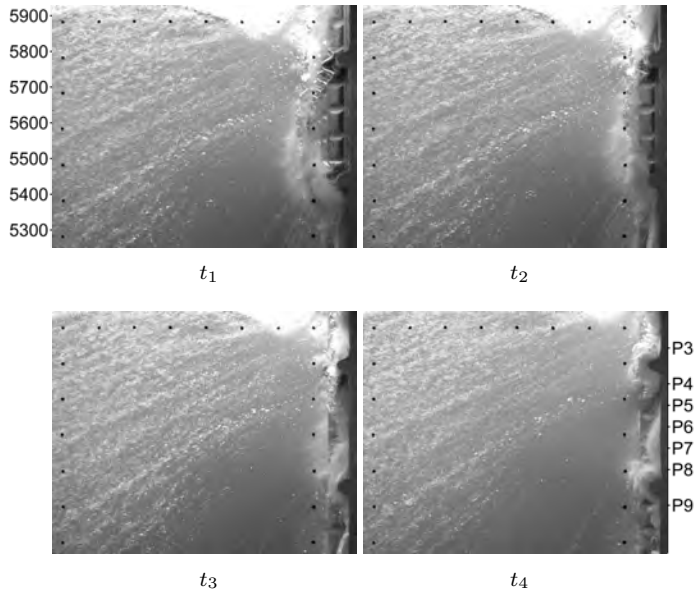

FIGURE 12: Flip-through impact on corrugated wall at four different instants. Time step equals 5 ms. Height given in millimeters.

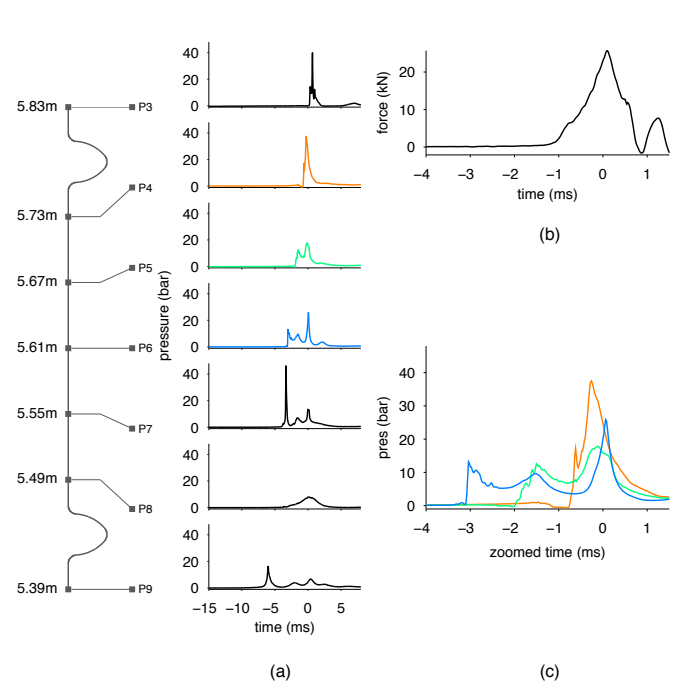

FIGURE 13: (a) Pressures, (b) Force on the bottom side of the horizontal corrugation in upward direction, (c) Zoom of pressures at sensors P4, P5 and P6.

the impact closing the pocket. This loading process is obviously an ELP3. After the impact due to the reattachment, a vertical jet builds up along the wall towards the upper corrugation. The root of the jet runs successively over sensors P6, P5 and P4. This jet can be seen on the image at t_4. Consequently, these sensor signals present a sharp rise of pressure one after the other. The loading process involved is the *building jet* ELP (ELP2). Only the first peak on the pressure signal of sensor P4 is due to ELP2. The interval between two successive rises of pressure is approximately 1 ms, which corresponds to a jet speed of 60 m/s.

Whatever the type of wave impact, the run-up of the trough keeps going after a reattachment and leads to an impact onto the lower side of the next corrugation. The violence of the impact depends on the vertical velocity of the trough. Therefore it is insignificant for a gas pocket impact, it is stronger when the conditions are closer to the flip-through impact. The loading process resulting from these impacts on the corrugation is the consequence of the discontinuity of velocity before and after the impact at the contact points. It is the *direct impact* ELP (ELP1). It is accompanied by a pressure wave emmitted downwards from the corrugation that will be felt by the sensors underneath the impacted corrugation as a remote influence of the impact.

For the slosh impact of Figure 10, the direct impact (ELP1) of the trough on the upper corrugation is recorded by pressure sensor P4 and the horizontal corrugation sensor around t_3. The maximum pressure recorded is close to 11 bar. The remote influence propagated by the pressure wave is clearly visible on pressure signals of sensors P5 and P6. The interval between the pressure peaks due to this pressure wave corresponds to a speed of the pressure wave of 270 m/s. This value corresponds to a speed of sound into aerated water for an aeration rate of 0.2% (see Minnaert (1933)).

For the flip-through impact of Figure 12, the direct impact (ELP1) of the trough on the upper corrugation is recorded by pressure sensor P4 and the horizontal corrugation sensor 1 ms before t_4. The maximum pressure is close to 38 bar. Only the sharp rise of the pressure signal, after the secondary peak, is due to ELP1. It has already been explained that the secondary peak was due to the building jet from the trough (ELP2) passing by P4. The comparison of the time traces of the force on the horizontal corrugation and of the pressure at P4 shows that the force starts increasing before the pressure. This is due to the jet from the trough hitting the corrugation before the root of the jet passes by P4. This proves that the second rise of the force and the second rise of the pressure at P4 are not only due to this thin jet but also due to the bulk of water at the trough level impacting the corrugation. The remote influence of the direct impact on the corrugation is clearly felt successively by sensors P5 and P6. The interval between the pressure peaks gives an evaluated speed of sound of 375 m/s which corresponds to an aeration rate of 0.1% (see Minnaert (1933)).

The rise of pressure due to ELP2 at P4 is very sharp and starts from zero. This shows that the gas above the trough can escape freely under the upper corrugation without any compression. The white cloud around the upper corrugation that can be distinguished on Figure 12 at t_4 is due to the spray induced by the quick flow of gas in between the corrugation and the free surface, namely the Kelvin-Helmholtz free surface instability (Drazin and Reid (2004)). However, in case of the slosh impact of Figure 10, there is a more progressive initial rise of the pressure at sensor P4. This indicates that the air below the corrugation is compressed during the approach of the trough, because it could not escape freely. Pressure sensor P4 thus captured first an ELP3 loading process.

Loads induced by the wave crest

When a wave crest directly impacts a horizontal corrugation, the load on both sides of the corrugation is small and the load on the flat area around the corrugation is mitigated compared to what would happen without the presence of the corrugation. When a wave crest impacts directly the flat area in between the corrugations the first phase of the impact is obviously the same as for a crest impact on a flat wall, with the same three different stages: (1) the approach forcing the gas to escape quickly, creating a spray around the tip of the crest; (2) the direct impacts (ELP1) at the contact points with the wall; (3) the vertical jets running upwards and downwards along the wall (ELP2). It may happen that during the approach the gas starts to be compressed (ELP3) as it cannot escape quickly enough. It may also happen that small gas pockets are entrapped between the multiple contact points of the crest generating high frequency oscillations of the pressure signals.

The crest impact described in Figure 14 takes place in between the horizontal corrugations. The spray in between the wall and the tip of the crest can clearly be seen at t_1. The first contacts occur in the vicinity of sensors P7 and P6 just after t_1. Sharp pressure peaks are observed in the pressure signals of P6 (around 3.5 bar) and P7 in Figure 15 just after t_1, as a consequence of the direct impacts (ELP1). Small amplitude and high frequency oscillations of the pressure signals can be distinguished just after the peaks due to the presence of a small gas pocket within the crest. This small gas pocket, separating the upward and the downward jets along the wall, can be seen in the image at t_3. The root of the downward jet passes by sensor P8 inducing a rise of the corresponding pressure signal (ELP2). The root of the upward jet passes successively by sensors P5 and P4 inducing the first rise of their corresponding pressure signals (ELP2). The time for the upward jet to go from P6 to P5 is about 3 ms, corresponding to a speed of 20 m/s.

After this first phase of a crest impact on a corrugated wall, the top of the crest keeps moving upwards, shortly preceded by the upward jet induced by the crest, until hitting the next horizontal corrugation. This direct impact (ELP1) induced by the crest on a horizontal corrugation is very similar to the direct impact induced by the trough on a

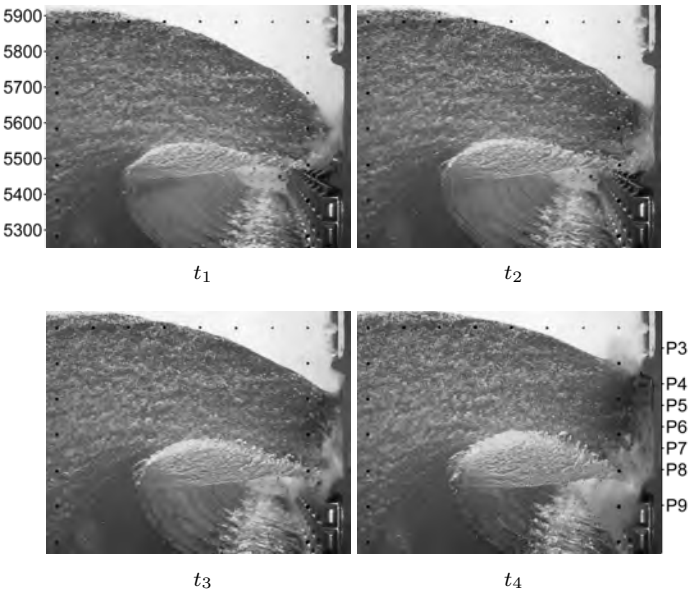

FIGURE 14: Air pocket impact on corrugated wall at four different instants. Time step equals 5 ms. Height given in millimeters.

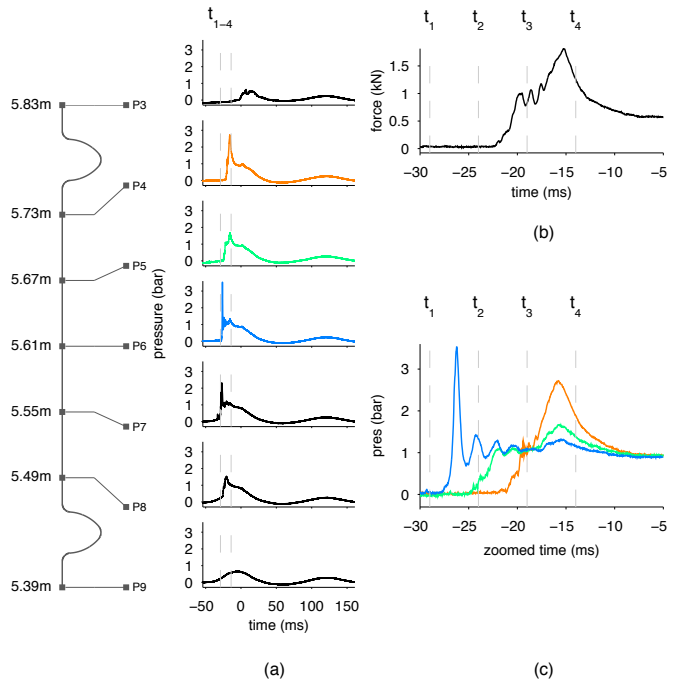

FIGURE 15: (a) Pressures, (b) Force on the bottom side of the horizontal corrugation in upward direction, (c) Zoom of pressures at sensors P4, P5 and P6.

horizontal corrugation. The discontinuity of vertical velocity imposed by the presence of the corrugation generates a pressure wave downwards the corrugation that is quickly damped but might still be felt a few tens of centimeters below the corrugation.

A close up view of this last phase (in between t_3 and t_4) of the crest impact of Figure 14 is given in Figure 16. The camera focused on the upper corrugation and captured the impact of the upward jet and of the close following bulk of the crest on the lower side of the corrugation. The force recorded by the lower part of the horizontal corrugation sensor, shown in Figure 15, presents a sharp peak due to this direct impact. The two parts in the force rise might be attributed respectively to the impact of the jet and then the impact of the liquid bulk. The second rise of the pressure signal at P4 is the consequence of this direct impact on the corrugation. Pressure sensors P5 and P6 also present small peaks almost at the same time as a remote influence of

this ELP due to the pressure wave.

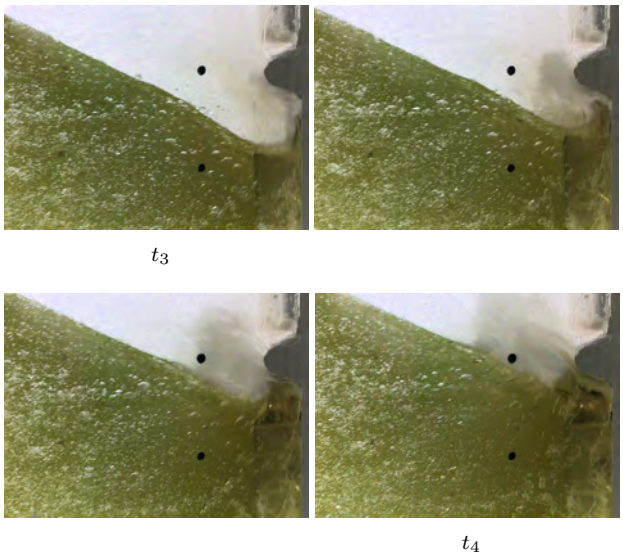

FIGURE 16: Close up of the jet from crest impacting the horizontal corrugation. The instants t_3 and t_4 refer to the same instants as in Figure 14. Time step equals 1.7 ms.

Loads induced by the entrapped air pocket

The presence of corrugations does not change the formation of air pockets significantly. It might, in certain conditions, prevent the gas from escaping as freely as with a flat wall and induce an earlier compression into the pocket and in front of the crest. Otherwise, the same oscillations of the gas pocket volume and pressure are expected with a corrugated wall as with a flat wall for the same incident wave. The *pulsating gas pocket ELP* (ELP3) applies on a part of the wall, but also on the sides of the corrugations, in contact with the gas pocket. Its remote influence on the wall below the pocket or inside the crest should also remain more or less the same as without corrugations. For the impact shown in Figure 14, only pressure sensor P9 remains inside the pocket from the beginning of its closure to the end of the signals shown in Figure 15. The pressure signal at P9 shows the typical damped oscillations of an ELP3. The beginning of the compression starts on P9 and P8 before the closure of the pocket, namely before the direct impacts at P7 and P6, which means that the gas is compressed while still escaping. The parallel behavior of the signals from P9 to P3 might be partially caused by a remote influence of the air pocket oscillations within the crest, at least before each sensor is enclosed one after the other into the upward moving pocket.

ELEMENTARY LOADING PROCESSES

Three Elementary Loading Processes have been identified in the previous sections as the building blocks of any load possibly induced by a breaking wave impact in a flume on a flat or on a corrugated wall. It means that any part of a pressure signal recorded on the wall or any part of a force signal recorded either on the wall or on a corrugation is considered as the result of one or a combination of these three ELPs. They are: the direct impact (ELP1), the building jet along the wall (ELP2) and the pulsating entrapped or escaping gas (ELP3). Moreover as each of these ELPs is directly related to one of the main physical phenomena involved in any liquid impact onto a structure, they are considered as the building blocks of any liquid impact load, including sloshing loads. The physical phenomena associated to the three ELPs are respectively: the pressure wave propagation through the liquid phase due to the liquid compressibility, the sharp change of liquid momentum direction in front of the wall and the pressure oscillations of the entrapped or escaping gas due to the gas compressibility. They interact with each other and with other physical phenomena involved during liquid impacts such as, the phase transition when liquid and gas phases are in thermodynamical equilibrium or the elasticity of the impacted structure. These other phenomena might influence significantly the three ELPs but are not sources of new kinds of ELPs. This section summarizes the characteristics of each ELP and the situations when they occur. It also describes the typical combinations of ELPs as observed during the Sloshel test campaigns.

Direct impact (ELP1)

When a moving volume of liquid meets a fixed structure, the liquid particles first in contact with the structure have their velocity component normal to the wall that is reduced to almost nothing in a very short time, depending on the compressibility of the liquid and the elasticity of the structure. This discontinuity of velocity at a contact point gives birth to a hemispherical pressure wave into the liquid and a hemispherical strain wave into the structure, both propagating at the speed of sound in the respective medium. These waves propagate with a quick attenuation due to the dissipation of the wave energy. For an ideally rigid structure, only the compressibility of the liquid is involved.

Direct impacts (ELP1) have been encountered during the Sloshel project in the following situations summarized in Table 1:

- Impact of a wave crest on a flat wall or in between two horizontal corrugations of a MarkIII membrane. This situation occurs for all gas pocket impacts including those with a very small one that could be considered as flip-through impacts.
- Impact of a reattaching trough. This situation happens for corrugated walls when the wave trough running-up along the wall separates from the wall due to the presence of a horizontal corrugation and reattaches to the wall above the corrugation, pushed by the close presence of the wave front.
- Impact of a jet on a horizontal corrugation. Such jets run up along a corrugated wall until hitting a horizontal corrugation. They are created by ELP2 (building jets) described in next paragraph.

ELP1 has not been studied much in the context of sloshing impacts. In Couty and Brosset (2000) simple liquid impact configurations were studied numerically. A column of liquid impacting a rigid structure with an initial velocity was simulated. A 1D analytical surrogate model giving a simple and quick overestimation of the maximum pressure due to ELP1 for any impacted sandwich structure was proposed.

The impulsive load induced by a direct impact is much localized and very short and might reach the acoustic pressure. Its main features depend on the initial impact velocity, the incidence of the impacting particles with regards to the wall and the shape of the liquid around the contact point. The specific loaded area associated to ELP1 is centred around the contact point and spreads out with the pressure wave at the local speed of sound until the pressure wave amplitude vanishes (remote influence). According to Sloshel results, the maximum radius of such specific loaded area is smaller than 200 mm. Within this loaded area the gradient of pressure is very strong and may vary of several bars in a few centimeters as in Figure 11 for the direct impact of the trough on the upper corrugation. The duration of such pressure distribution on the whole specific loaded area is typically shorter than 1 ms. It is even shorter at the location of a fixed pressure sensor. Most of the time, when this ELP is detected by pressure sensors, the sensor is not located exactly at the center of the specific loaded area and does not capture the maximum pressure.

Although ELP1 is so momentary, its influence is felt locally by the structure. For instance a direct impact on a MarkIII panel is felt by the top plywood of the containment system as it has been shown in Brosset et al. (2011) for a flip-through impact in the last Sloshel campaign. Strain gauges located behind the top plywood plate of the MarkIII

panel are more likely to record a strain peak than pressure sensors to record a pressure peak under the influence of ELP1, because the structural behavior is necessarily more global.

Building jet (ELP2)

Even when considered as ideally incompressible, a liquid moving in a tank induces hydrodynamic loads on the walls. The restoring force exerted locally by the wall on the liquid forces the liquid to turn and respect the boundary condition. There are a few situations for which these loads can be significant. These situations are always associated with the birth of a jet along the wall, they are the ELP2 conditions.

Building jets (ELP2) have been encountered during the Sloshel project for the following situations summarized in Table 1:

- Jets induced by any direct impact. As described previously, such direct impact may be caused by a crest either on a flat wall or in between two horizontal corrugations. It may also be caused by a reattaching trough on a corrugated wall. Theoretically, it may also develop over an impacted corrugation by a jet. In that case, a secondary jet flows over the corrugation (as on Figure 16) starting from the root of the corrugation. ELP2's signature could unfortunately not been discriminated from ELP1's during the Sloshel tests, as no pressure sensors were put directly on the corrugations. Whatever the direct impact, which is the source for ELP2, two jets are induced from the impact area: an upward jet and a downward jet.
- Jet induced by a restricted trough. When the trough is restricted by the close presence of the wave front (situation close to a flip-through impact), the situation may lead to the creation of an upward jet.

Whatever the condition giving birth to a liquid jet along the wall, there is a sharp gradient of pressure at the root of the jet where the liquid flow has to turn abruptly. The pressure pulse travels with the root of the jet and fades with the jet intensity. This intensity depends on the possibility for the local flow to feed the jet and on the angle value between the free surface (without the extension of the jet) and the wall. The smaller this angle, the sharper the change of local liquid momentum but also the stronger the interaction with the gas which might mitigate the input conditions of ELP2.

As the pressure pulse induced by ELP2 is travelling with the root of the jet at a velocity V_J, the average pressure recorded instantenously by a sensor at a fixed location depends on both V_J and the size of the sensitive part of the sensor. The smaller the sensor the higher the pressures. The relevant duration for the dynamic analysis of a structure submitted to such an ELP is expected to be derived from V_J and from a characteristic dimension of the expected mode and not from the duration of a recorded peak pressure.

ELP2 has been studied experimentally much, especially by means of drop tests of wedges on a water free surface initially at rest (see for instance Zhao and Faltinsen (1993)). As for such drop tests with a deadrise angle of the wedge larger than 6 degrees, the gas can escape easily when the wedge approaches the free surface, there is almost no interaction between the wedge and the gas. Moreover the velocity of the escaping gas is not high enough to create wavelets on the water free surface. Therefore, ELP2 is the only Elementary Loading Process involved in such cases. This explains why ELP2 has often been considered as the only component of impact loads. Such drop-tests are ideal situations for studying ELP2: the recorded impact pressures repeat accurately and compare rather well with theoretical approximations as the one proposed in Wagner (1932). ELP2 is the only Elementary Loading Process that might be, at best, captured by numerical simulations with incompressible fluids. The difficulty for CFD lies in the multi-scale problem: capturing both the global flow for a large domain (characteristic size ranges from one meter for a drop-test to a few tens of meters for a wave impact in a flume or for a sloshing impact in a tank of a LNG carrier) and very local pressures (characteristic size = 1 mm).

Pulsating entrapped gas (ELP3)

There are several possibilities for the gas compressibility to play a direct role in the loading induced by wave impacts. The gas may be completely entrapped in a pocket or still escaping in between the wall and the approaching wave avoiding, at least partially, the entrapment or allowing a leakage from the pocket. If the gas is compressed when escaping during the wave approach, it means that the escaping velocity is not large enough for the gas to keep the initial density. The compression is often assumed to start around Mach 0.3, namely for air velocities larger than 100 m/s. Only when the pocket is closed, even though leakage occurs, is the pressure on the wall significant. Entrapped or escaping, the compressibility provides a stiffness to the gas.

Situations witnessed during the Sloshel project for escaping gas to be compressed turn out to be the same as for ELP2 to occur: just before a direct impact (crest or reattaching trough) or for a restricted trough condition. The compression is not significant but still can be observed before the complete entrappment of any air pocket. The most important aspect of this compression of escaping gas is to mitigate the possible following direct impact and to create a spray around the free surface because of the Kelvin-Helmholtz instability. This is typically what is observed during drop-tests of a wedge with a small deadrise angle.

Situations witnessed during Sloshel project for complete gas entrapment are listed below and summarized in Table 1:

- Gas pockets closed by a direct impact. Such direct impact may be caused by a crest either on a flat wall or in between two horizontal corrugations (*gas pockets closed by a crest*). In that case the pocket is enclosed by the wave (trough, front and crest) and the wall. The size of the pocket, for a given liquid height at rest, depends on the distance between the point were the wave starts breaking and the wall. Such direct impact may also be caused by a reattaching trough on a corrugated wall (*gas pockets closed by a reattaching trough*). In that case a small pocket is created above the horizontal corrugation that caused the flow separation from the wall and below the reattachment point. It may also be caused by the impact of an upward jet on the lower side of a horizontal corrugation. In that case the small deflection of the MarkIII foam together with the slight downward rotation of the corrugation favors the gas entrapment as shown in Brosset et al. (2011).
- Small gas pockets enclosed directly by a wave crest and the wall. This should also happen with a reattaching trough, but this has not been clearly seen during the Sloshel tests.

The pressure within a gas pocket can be considered as uniform. Indeed, the pressure sensors within a given pocket record almost the same pressure signals. The pressure time history always shows damped oscillations which correspond to the pulsations of the pocket volume. These oscillations can be considered as the signature of ELP3. They look similar to those obtained with any mass/spring/damper system. During the expansion of the pocket, the pressure inside the pocket may decrease below the atmospheric pressure. For gas pockets directly entrapped by a gas-pocket type of wave impact in a flume, the smaller the pocket, the higher the pressure and the frequency of oscillations. In such a case the period of the oscillations is large compared to the *duration* of an ELP1 or an ELP2 (whatever definition is given to this *duration*). The specific loaded area of an ELP3 does not only cover the surface of the gas pocket on the wall. Indeed, there is a remote influence which is felt on wetted points of the wall. Obviously, the closer these points are to the pocket, the larger the influence. Typically when a pressure signal recorded during a gas pocket impact presents some parts that are in phase with the signals recorded within the gas pocket but with a smaller amplitude, this is due to the remote influence of the pocket pulsation. Because of this remote influence ELP3 will often cumulate with one of the other ELPs. For example, the pressure at a point of the wall surface, which

TABLE 1: Simplified list of situations for each ELP to occur

Loading	Flat wall	Corrugated wall
Direct impact	Crest	Crest
		Reattaching trough
		Jet on corrugation
Building jet	Crest	Crest
		Reattaching trough
	Restricted trough	Restricted trough*
Pulsating entrapped air	Closed by Crest	Closed by Crest
		Closed by Reattaching trough
		Closed by Jet on corrugation
	Enclosed by Crest	Enclosed by Crest

*note that this has not been observed at full scale

is just under the root of a downward jet induced by a crest impact, cumulates the remote influence of the gas pocket pressure (ELP3) and the building jet pressure (ELP2).

Most of the time, but not always, the part of the local pressure due to ELP3 is small (but still significant) with regards to the part due to either ELP1 or ELP2. On the contrary, as the specific loaded area of pulsating air pockets including its remote influence may be large compared to the characteritic size of a MarkIII panel, the global force induced by the compression of large gas pockets on a MarkIII panel are among the highest. Consequently, ELP3 must not be neglected from a structural point of view.

Semi-analytical and numerical models have been proposed to study the behavior of entrapped gas pockets. Bagnold (see Bagnold (1939)) proposed first a 1D semi-analytical piston model which is ruled by two dimensionless numbers: the adiabatic constant of the gas and the *impact number* (initial kinetic energy of the piston divided by the ullage pressure times the initial length of the pocket). This model does not include any energy dissipation. Therefore, the calculated volume and pressure oscillations are not damped. This model has been used by Bogaert, Léonard, Brosset and Kaminski (2010) to address the scaling issue for the pressures inside gas pockets and their oscillation frequencies. This model has been enhanced by Braeunig et al. (2010) in order to include the phase transition phenomenon. In Guilcher et al. (2010), an air-pocket wave impact in a flume is simulated thanks to a mixed Boundary-Element-Method/Smoothed-Particle-Hydrodynamics approach. The simulation was performed until the pressure into the pocket becomes lower than the atmospheric pressure and a numerical instability develops. In Abrahamsen (2011) a simulation of a *Sloshing induced tank-roof impact with entrapped air pocket* is proposed. A method referred to as the Boundary-Element/Finite-Difference method is used to simulate the flow until the wave hits the roof. The oscillation stage is simulated by a method referred to as the mixed Eulerian-Lagrangian method. The calculated first pressure maximum and frequency of the oscillations compare rather well with the experimental results. Only the damping coefficient is underestimated.

Physical phenomena related to ELPs - Typical combinations of ELPs

Each ELP is related to a main governing phenomenon: liquid compressibility for ELP1, change of liquid momentum for ELP2 and gas compressibility for ELP3. Nevertheless, other physical phenomena involved during a liquid impact may interfere. For instance each ELP interacts with the elasticity of the impacted structure (hydroelasticity). Moreover if the gas involved is the vapor of the liquid in thermodynamical conditions close to the equilibrium, the condensation of the gas will interact with ELP3. It has also been observed that the Rayleigh-Taylor instability of the free surface may develop in case of an ELP3 for an entrapped gas pocket, contributing to damping of the oscillations.

Before any impact, the phase of gas escaping in between an approaching wave and a wall can be split in two stages. At first the gas escapes almost freely and the flow can be considered as incompressible. A transfer of momentum between the liquid and the gas intervenes which is ruled by the Density Ratio between gas and liquid. The flow of escaping gas accelerates and creates instabilities at the free surface (Kelvin-Helmholtz). At a certain moment the gas cannot escape quickly enough to keep the same density in the remaining volume in between the wave and the wall, the compression starts. For the sake of clarity, as this second stage of the gas escaping is related to gas compressibility, the associated Elementary Loading Process has been grouped with ELP3. A specific ELP (e.g. ELP0) could have been defined as well, for the list of associated physical phenomena, including the transfer of momentum from the liquid to the gas and Kelvin-Helmholtz, is not the same as for an ELP3 caused by an entrapped gas pocket.

A temporal and spacial load distribution correspond to any liquid impact on a wall. This distribution may, in certain academic situations, result from an unique ELP as, for instance, the load induced by the drop of a wedge on a water free surface initially at rest (ELP2). Normally, the load distribution results from a combination of ELPs. The most typical combination of ELPs corresponds to: 1. ELP3, while the gas tries to escape during the approach of the wave; 2. ELP1, for any type of direct impact; 3. ELP2, building jet(s) induced by the direct impact + ELP3, pulsating gas pocket after entrapment is achieved due to the direct impact. This typical combination of ELPs together with their related physical phenomena is represented schematically in Figure 17.

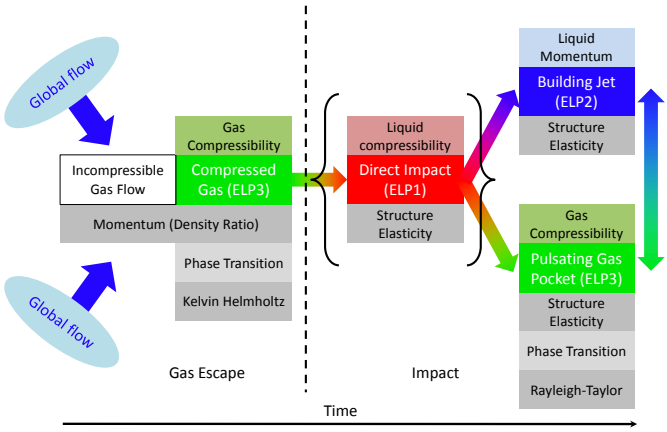

FIGURE 17: Typical combination of ELPs - Associated physical phenomena

Most of the time it involves a direct impact but the combination can also exist without the direct impact in case of a trough run-up strongly restricted by a close wave front, which explains why the Direct Impact ELP is represented between brackets in the figure.

This combination of ELPS occurs, at least partly, in many situations:

- When a gas-pocket wave impact occurs onto a flat or a corrugated wall. In that case, the direct impact (ELP1) is caused by the wave crest;
- When the wave trough reattaches to the wall (ELP1) after separation over a horizontal corrugation during the run-up process;
- When a jet induced by a first direct impact hits a horizontal corrugation;
- During the run-up of a restricted trough along a flat wall, even when no direct impact is involved.

ELPs and scaling

In the context of sloshing, model tests are performed at small geometrical scale $1 : \lambda$ (most of the time $\lambda = 40$). The imposed motions

are down scaled from scale 1 according to both the geometrical scale and an associated time scale $1 : \sqrt{\lambda}$, in order to keep the same Froude number at both scales. Model tests are performed with water and a heavy gas so that the density ratio between the gas and the liquid matches the range on board LNG carriers (around 0.004). This condition actually corresponds to a mass scaling. The model tank walls are flat and rigid (for a more complete description of model tests carried out for a sloshing assessment, see Gervaise et al. (2009)). Scaling the measured pressures to full scale includes several combined issues that the notion of ELP helps to unravel:

- **Three Elementary Loading Processes are involved at both scales during the impacts but two of them, ELP1 and ELP3, are associated with physical phenomena which do not follow Froude scaling**. Indeed, as ELP2 is related to liquid change of momentum, considered separately, it should Froude scale. Unfortunately, as ELP1 is related primarily to liquid compressibility and ELP3 is related primarily to gas compressibility, the liquid and gas at model scale should have their respective compressibility adequately down scaled from the properties of respectively Liquefied Natural Gas (LNG) and Natural Gas (NG) in order to allow a Froude scaling for the pressure when the input conditions (Global flow) are Froude scaled. This corresponds at first approximation to Froude scaling the speeds of sound in LNG and NG as explained in Braeunig et al. (2009). This is physically impossible as it would lead to unrealistic values for a liquid or a gas. Therefore liquid and gas compressibility biases are bound to happen. The bias amplitude depends on the time-space distribution of the ELPs for each impact.
- **Some physical phenomena included during impacts at full scale are not taken into account at model scale**. These phenomena are mainly the phase transition and the elasticity of the impacted structure. They are not able to generate dedicated ELPs but will interact with the phenomena associated to the three classical ELPs and therefore modify the intensity of each ELP and the interaction between them.
- **As the tank walls of the model tanks are flat, some situations where the bulges of the membrane (corrugations of MarkIII or raised edges of NO96) would generate combinations of ELPs at full scale are not taken into account at model scale**. These situations, as can be checked in Table 1 when comparing the sources of ELPs on a flat wall and on a corrugated wall, are the consequence to either the reattachment of the flow after separation on a horizontal corrugation during the trough run-up or the impact of a vertical jet along the wall on a horizontal corrugation. Even when the sources of ELPs are of the same kind on a flat or a corrugated wall (consequence of a crest impact or a restricted trough), the input conditions would be different, mainly because of the different ways for the gas to escape before the impact.

CONCLUSIONS

The interactions between breaking waves and a flat or a corrugated wall have been investigated in this paper. The analysis was carried out based on the experimental results from the Sloshel project. The interactions between the different parts of the waves and the corrugated wall were identified from the *full scale MarkIII tests*. The interactions between the different parts of the waves and the flat wall were identified from tests at scale 1:6, so-called *large scale tests*. Only the qualitative results related to the phenomenology are reported in this paper. The quantitative results and the direct consequences on a sloshing assessment methodology based on model tests are presented in Marhem et al. (2012).

Three Elementary Loading Processes (ELP) have been identified when a breaking wave impacts a flat or a corrugated wall: the direct impact (ELP1), the building jet (ELP2) and the compression/expansion of entrapped or escaping gas (ELP3). The time and space distribution of pressures on the impacted wall is always a combination of these three ELPs, which have distinguishable pressure signatures. The interactions between the breaking waves and the flat or the corrugated wall are sources for different combinations of these ELPs. Additional sources for ELP combinations are provided by the presence of corrugations that would obviously not exist with a flat wall. They are mainly the consequence of (1) the reattachment of the flow to the wall after separation from a horizontal corrugation during the trough run-up or (2) the impact of a horizontal corrugation by a vertical jet running along the wall. The interactions between a wave and the horizontal raised edges of the N096 membrane would induce similar additional sources for ELP combinations. The sources of ELPs that are common for a flat and a corrugated wall are either the consequence of a crest impact or a restricted trough run-up. Even for those cases which look very similar in nature whatever the wall surface, the resulting loading might be significantly different because the phase of gas escaping before the impact would be different and the global run-up speed would also be different, inducing thus different input conditions for the similar ELPs.

Each of the three ELPs is associated with a different *primary* local physical phenomenon: liquid compressibility for ELP1, change of liquid momentum for ELP2 and gas compressibility for ELP3. Taken separately, each ELP would therefore scale differently when considering Froude-similar impact inflow conditions at two different scales. ELP2 is expected to Froude-scale when considered alone. ELP1 and ELP3 are expected to Froude scale only if respectively the liquid and gas compressibilities are adequately scaled, which is not possible for sloshing model tests as it would request unrealistic fluids at model scale. How to scale adequately typical combinations of ELPs is today an open question addressed by GTT by studying idealized impacts by means of experiments, numerical simulations or semi-analytical models.

How much the lack of physics in the sloshing model tests spoils a simple Froude scaling of the measured pressures for deriving design pressures is a question addressed by several R&D projects GTT is involved in. One of them consists in comparing sloshing model tests of a slice of the tank #2 of a membrane 150,000 m^3 LNG carrier at three different scales (1:10, 1:20 and 1:40). Only tests at scale 1:10 have been performed so far. The results are presented in Brosset et al. (2012). Another consists of comparing Sloshing model tests at scale 1:40 and 1:25 to Full Scale Measurements carried out on board a 148,000 m^3 LNG carrier. The results are presented in Berthon and Pasquier (2012).

For the time being GTT uses empirical scaling factors derived from the feedback at sea, namely from the knowledge that can be drawn from real sloshing incidents on board LNG carriers. Sloshing model tests have been performed in order to mimic accurately real voyages that led to a certain amount of (slightly) damaged insulation panels or boxes in LNG carriers. The empirical scaling factors are fitted in order the probability of failure derived from GTT's sloshing assessment methodology matches the real ones.

REFERENCES

Abrahamsen, B. (2011). Sloshing induced tank-roof impact with entrapped air pocket, *PhD Thesis, NTNU Norwegian University of Science and Technology*.

Bagnold, R. (1939). Interim report on wave-pressure research, *J. Inst Civil Eng.* **12**: 201–226.

Berthon, C. and Pasquier, R. (2012). Model Scale Tests vs. Full Scale Measurement: findings from the Full Scale Measurement of Sloshing project, *Proceedings of 22th International Offshore and Polar Engineering Conference, June 17-22, Rodos, Greece*.

Bogaert, H., Brosset, L. and Kaminski, M. (2010). Interaction between wave impacts and corrugations of MarkIII membrane: findings from the Sloshel project, *Proceedings of 20th International Offshore and Polar Engineering Conference, June 20-26, Beijing, China*.

Bogaert, H., Léonard, S., Brosset, L. and Kaminski, M. (2010). Sloshing and scaling: results from Sloshel project, *Proceedings of 20th International Offshore and Polar Engineering Conference, June 20-26, Beijing, China*.

Braeunig, J., Brosset, L., Dias, F. and Ghidaglia, J. (2009). Phenomenological study of liquid impacts trough 2D compressible two-fluid numerical simulations, *Proceedings of 19th International Offshore and Polar Engineering Conference, June 21-26, Osaka, Japan*.

Braeunig, J., Brosset, L., Dias, F. and Ghidaglia, J. (2010). On the effect of phase transition on impact pressures due to sloshing, *Proceedings of 20th International Offshore and Polar Engineering Conference, June 20-26, Beijing, China*.

Brosset, L., Karimi, R., Kosinski, C. and Amaichan, J. (2012). Sloshing Model Tests at scale 1:10, *Proceedings of 22th International Offshore and Polar Engineering Conference, June 17-22, Rodos, Greece*.

Brosset, L., Lafeber, W., Bogaert, H., Marhem, M., Carden, E. P. and Maguire, J. R. (2011). A MarkIII panel subjected to a Flip-trough impact: Results from the Sloshel project, *Proceedings of 21th International Offshore and Polar Engineering Conference, June 19-24, Hawaii, USA*.

Brosset, L., Mravak, Z., Kaminski, M., Collins, S. and Finnigan, T. (2009). Overview of Sloshel project, *Proceedings of 19th International Offshore and Polar Engineering Conference, June 21-26, Osaka, Japan*.

Couty, N. and Brosset, L. (2000). 3D numerical simulation of sloshing impacts including fluid-structure interaction, *Proceedings of the International Conference on Ship and Shipping Research, NAV2000, September 19-22, 2000, Venice, Italy*.

Drazin, P. G. and Reid, W. H. (2004). Hydrodynamic stability, *Cambridge University Press*.

Gervaise, E., de Sèze, P. and Maillard, S. (2009). Reliability-based methodology for sloshing assessment of membrane LNG vessels, *Proceedings of 19th International Offshore and Polar Engineering Conference, June 21-26, Osaka, Japan*.

Guilcher, P.-M., Oger, G., Brosset, L., Jacquin, E., Grenier, N. and Touze, D. L. (2010). Simulation of liquid impacts with a two-phase parallel SPH model, *Proceedings of 20th International Offshore and Polar Engineering Conference, June 20-26, Beijing, China*.

Kaminski, M. and Bogaert, H. (2010a). Full-Scale Sloshing Impact Tests Part I, *International Journal of Offshore and Polar Engineering* **20**: 1–10.

Kaminski, M. and Bogaert, H. (2010b). Full-Scale Sloshing Impact Tests Part II, *Proceedings of 20th International Offshore and Polar Engineering Conference, June 20-26, Beijing, China*.

Kimmoun, O., Ratouis, A. and Brosset, L. (2010). Sloshing and scaling: Experimental Study in a Wave Canal at Two Different Scales, *Proceedings of 20th International Offshore and Polar Engineering Conference, June 20-26, Beijing, China*.

Marhem, M., Lafeber, W., Bogaert, H. and Brosset, L. (2012). Loads on MarkIII corrugated primary membrane: findings from the Sloshel project, *Proceedings of 22th International Offshore and Polar Engineering Conference, June 17-22, Rodos, Greece*.

Minnaert, M. (1933). Musical air bubbles and the sound of running water, *Phil. Mag.* **16**: 235–248.

Wagner, H. (1932). ber stoss- und gleitvorgange and der oberflache von flussigkeiten, *Z. Angew. Math. Mech.* **12**: 193–215.

Zhao, R. and Faltinsen, O. (1993). Water entry of two-dimensional bodies, *Journal of Fluid Mechanics* **246**: 593–612.

ACKNOWLEDGEMENTS

The authors would like to acknowledge the support provided by the Sloshel consortium members that have made the Sloshel project possible: American Bureau of Shipping, Bureau Veritas, Ecole Centrale Marseille, Chevron, ClassNK, Det Norske Veritas, GDF SUEZ, GTT, Lloyd's Register, MARIN, Total and Shell.

The views expressed in the paper are those of the authors and do not necessarily represent the unanimous views of all the consortium members.